ISSN 1063-7834, Physics of the Solid State, 2012, Vol. 54, No. 10, pp. 2005–2014. © Pleiades Publishing, Ltd., 2012.
Original Russian Text © S.S. Aplesnin, L.V. Udod, M.N. Sitnikov, D.A. Velikanov, M.V. Gorev, M.S. Molokeev, A.I. Galyas, K.I. Yanushkevich, 2012, published in Fizika Tverdogo Tela, 2012, Vol. 54, No. 10, pp. 1882–1890.

MAGNETISM

Magnetic and Electrical Properties of Bismuth Cobaltite $Bi_{24}(CoBi)O_{40}$ with Charge Ordering

S. S. Aplesnin[a, b, *], L. V. Udod[a, b], M. N. Sitnikov[a], D. A. Velikanov[b, c], M. V. Gorev[b, c], M. S. Molokeev[b], A. I. Galyas[d], and K. I. Yanushkevich[d]

[a] *Reshetnev Siberian State Aerospace University, pr. imeni Gazety "Krasnoyarskii Rabochii" 31, Krasnoyarsk, 660014 Russia*

[b] *Kirensky Institute of Physics, Siberian Branch of the Russian Academy of Sciences, Akademgorodok 50–38, Krasnoyarsk, 660036 Russia*

* *e-mail: apl@iph.rkasn.ru*

[c] *Siberian Federal University, pr. Svobodnyi 79, Krasnoyarsk, 660041 Russia*

[d] *Scientific–Practical Materials Research Centre, National Academy of Sciences of Belarus, ul. Petrusya Brovki 19, Minsk, 220072 Belarus*

Received January 11, 2012; in final form, March 21, 2012

Abstract—The compound $Bi_{24}(CoBi)O_{40}$ has been synthesized using the solid-phase reaction method. The temperature and field dependences of the magnetic moment in the temperature range $4\ K < T < 300\ K$ and the temperature dependences of the EPR line width and g-factor at temperatures $80\ K < T < 300\ K$ have been investigated. The electrical resistivity and thermoelectric power have been measured in the temperature range $100\ K < T < 1000\ K$. The activation energy has been determined and the crossover of the thermoelectric power from the phonon mechanism to the electron mechanism with variations in the temperature has been observed. The thermal expansion coefficient of the samples has been measured in the temperature range $300\ K < T < 1000\ K$ and the qualitative agreement with the temperature behavior of the electrical resistivity has been achieved. The electrical and structural properties of the compound have been explained in the framework of the model of the electronic-structure transition with inclusion of the exchange and Coulomb interactions between electrons and the electron–phonon interaction.

DOI: 10.1134/S106378341210006X

1. INTRODUCTION

Mixed-valence compounds exhibit remarkable magnetic and electrical properties. An example is provided by the manganites $La_{1-x}A_xMnO_3$ (A = Sr, Ca, Ba) [1, 2] with orbital, spin, and charge ordering. The well-studied iron oxides Fe_3O_4 [3, 4] with charge ordering in the magnetically ordered region are characterized by a high electrical conductivity, in particular, due to the closely spaced divalent and trivalent iron ions in octahedral positions. Cobalt oxide Co_3O_4 [5] and manganese oxide Mn_3O_4 [6] exhibit a low electrical conductivity, which is associated with the difference in the crystal structures, because the dominant contribution to the kinetic properties of the compound comes from the hopping of electrons between the cations in tetrahedral and octahedral sites. The magnetic and electrical properties of these compounds with charge ordering are determined by electrons of 3d metals. Charge ordering can be observed as a result of the removal of the orbital degeneracy of electrons in the 3d states due to the spin–orbit interaction and interaction with the phonon modes. The basic mechanism that is responsible for the charge ordering in these systems is rather difficult to determine. In order to get rid of the accompanying interactions and to describe the charge ordering as a transition in the electronic system, we consider electrons in the s states of the $Bi_{24}(CoBi)O_{40}$ compound containing the bismuth ions either with the filled $6s^2$ shell or with the empty 6s shell. The destruction of the charge ordering can lead to an electronic-structure transition and a change in the kinetic properties of the material.

The purpose of this work was to establish a correlation of the magnetic, electrical, and structural characteristics of the semiconductor with charge ordering.

2. SYNTHESIS AND CRYSTAL STRUCTURE

Polycrystalline bismuth cobaltite was synthesized by the solid-phase reaction method. The initial components, namely, bismuth oxide Bi_2O_3 and cobalt oxide Co_3O_4 of high-purity grade (99.9%), were carefully ground in an agate mortar. The powder thus obtained was pressed into pellets. The synthesis was carried out at a maximum temperature of 1023 K in several stages with intermediate grinding.

The X-ray powder diffraction pattern of the compound under investigation was recorded at room tem-

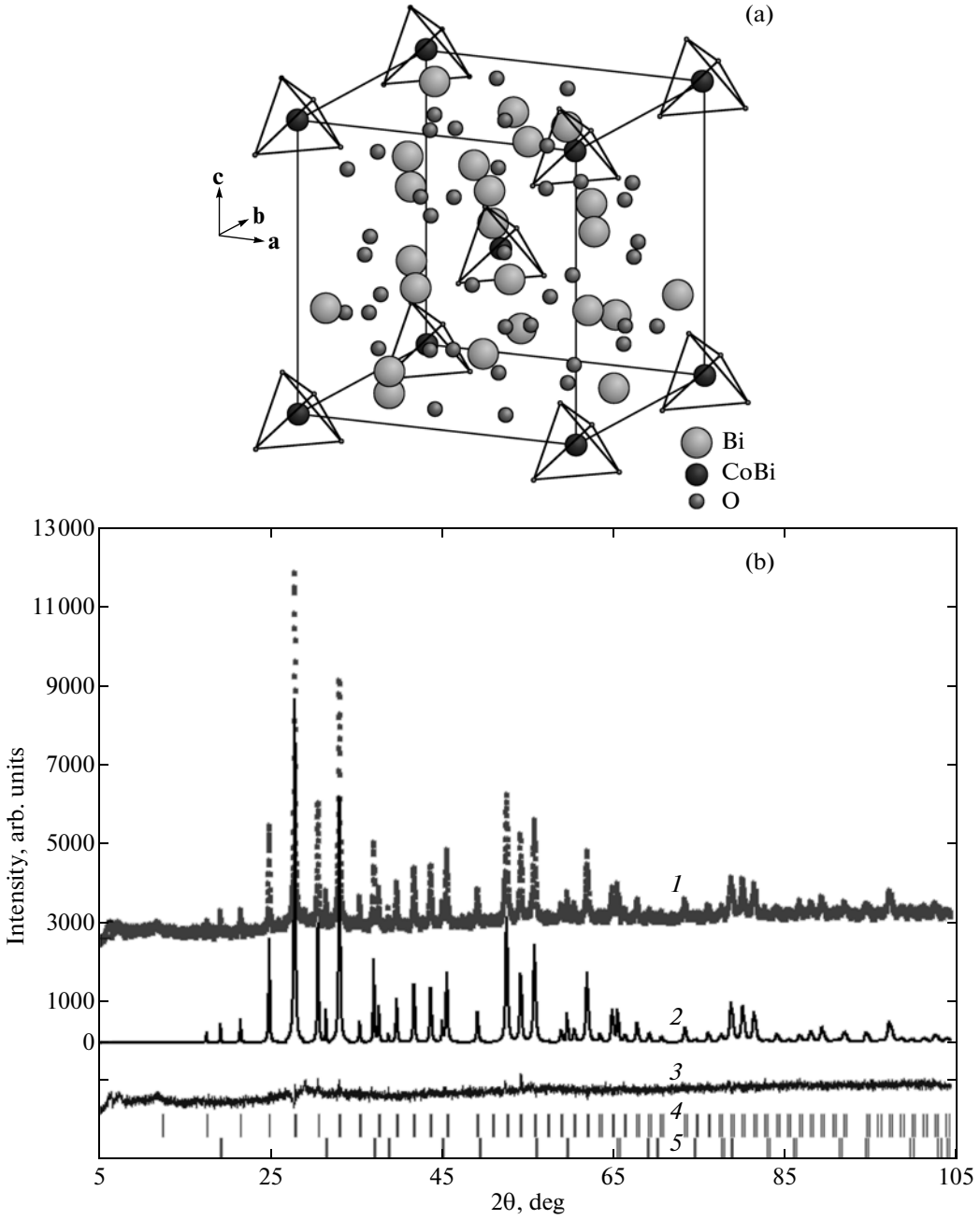

Fig. 1. (a) Crystal structure of the $Bi_{24}(CoBi)O_{40}$ compound. (b) X-ray powder diffraction pattern of the $Bi_{24}(CoBi)O_{40}$ sample: (*1*) experimental curve, (*2*) theoretical X-ray diffraction pattern, (*3*) difference between the experimental and theoretical X-ray diffraction patterns, (*4*) $Bi_{24}(CoBi)O_{40}$ phase, and (*5*) Co_3O_4 phase.

perature on a Bruker D8 ADVANCE X-ray powder diffractometer (CuK_α radiation, θ–2θ scan mode) equipped with a VANTEC linear detector. The 2θ scan step was 0.016°, and the exposure time per step was 0.6 s. The positions of all reflections were determined with the EVA program included in the DIFFRAC-PLUS software package (Bruker AXS, Germany). The X-ray powder diffraction analysis of the sample revealed that the synthesized compound consists of two phases: $Bi_{24}(CoBi)O_{40}$ and Co_3O_4. The main phase $Bi_{24}(CoBi)O_{40}$ has a cubic symmetry, which corresponds to the non-centrosymmetric space group $I23$ [7]. The unit cell contains one formula unit. The crystal structure of the $Bi_{24}(CoBi)O_{40}$ compound is shown in Fig. 1a. Two structurally nonequivalent bismuth atoms, Bi(1) and Bi(2), occupy the following positions: the Bi(1) atom occupies the position 24*f*, and the Bi(2) atom occupies the position 2*a*. The cobalt

atom occupies the same position 2*a* as the Bi(2) atom with a probability of 50%. The oxygen atoms O(1) and O(3) are located in the position 8*c*, and the O(2) atom occupies the position 24*f*. The bismuth atom Bi(2) and the cobalt atom are located in the tetrahedral environment formed by the oxygen atoms. The impurity phase Co_3O_4 has the structure of cubic normal spinel with the lattice parameter $a = 8.09$ Å [5, 8]. The refinement of the structures, unit cell parameters, profiles of the diffraction peaks, and contents of the phases in the sample was performed with the DDM program [9]. The result of the refinement is presented in Fig. 1b. The profile *R*-factor was $R_{DDM} = 8.49\%$, and the integrated *R*-factors were as follows: $R_B = 5.54\%$ for the $Bi_{24}(CoBi)O_{40}$ phase and $R_B = 5.43\%$ for the Co_3O_4 phase. The unit cell parameters after the refinement were as follows: $a = 10.1917(1)$ Å for the $Bi_{24}(CoBi)O_{40}$ phase and $a = 8.0842(1)$ Å for the Co_3O_4 phase. The contents of the phases in the sample were found to be as follows: 77.0(5)% for the $Bi_{24}(CoBi)O_{40}$ phase and 23.0(5)% for the Co_3O_4 phase.

The synthesis of pure samples of the $Bi_{24}(CoBi)O_{40}$ compound is a very difficult task because of the complex phase diagram of the Bi_2O_3–Co_3O_4 system (components allow for the formation of other compounds) and the volatility of Bi_2O_3 above its melting point. The same problems are encountered in the synthesis of the $BiFeO_3$ compound [10, 11]. In this paper, for comparison, we have presented the magnetic and electrical properties of the $0.77Bi_{24}(CoBi)O_{40} \cdot 0.23Co_3O_4$ and Co_3O_4 samples and the magnetic properties of the $Bi_{24}(CoBi)O_{40}$ compound.

The differential thermal analysis curve has no anomaly up to the temperature $T = 1157$ K. This indicates the absence of phase transitions in the material.

3. MAGNETIC PROPERTIES

The magnetic properties of the samples were investigated on a Quantum Design MPMS XL SQUID magnetometer in the temperature range 4 K < *T* < 300 K during heating at a rate of 4 K/min. The temperature dependences of the magnetic susceptibility measured for the two-phase compound $0.77Bi_{24}(CoBi)O_{40} \cdot 0.23Co_3O_4$ and the cobalt oxide Co_3O_4 in a magnetic field $H = 5$ T are shown in Fig. 2. The curve of the magnetic susceptibility of the cobalt oxide has a maximum near the temperature $T_{\chi max} = 39$ K, and the maximum of the derivative $d\chi/dT$ is observed at $T = 32$ K. The magnetic properties of the Co_3O_4 phase are well understood. According to some authors, the temperature $T_{\chi max}$ can be identified with the Néel temperature $T_N \approx 40$ K [12], whereas the others authors identify this temperature with the temperature of the maximum of the derivative $d\chi/dT$ [11]. The magnetic susceptibility χ_1 of the $Bi_{24}(CoBi)O_{40}$ phase was found by subtracting the magnetic susceptibility of the cobalt oxide χ_2 (taking into account the weight ratio) from the magnetic susceptibility of the two-phase compound χ: $\chi_1 = \chi - 0.23\chi_2$. Figure 2 also shows the temperature dependence of the reciprocal of the magnetic susceptibility $1/\chi_1$ for the $Bi_{24}(CoBi)O_{40}$ phase in the temperature range 4 K < *T* < 300 K, which is fairly well described by the Curie–Weiss law with the negative paramagnetic Curie temperature $\Theta = -12.3$ K and the effective magnetic moment $\mu = 5.08\ \mu_B$. Based on these data, we can assume that the magnetic moment of the $Bi_{24}(CoBi)O_{40}$ phase is determined by the spins of the trivalent cobalt ions located in tetrahedral positions with $S = 2$. The absence of long-range magnetic order for the $Bi_{24}(CoBi)O_{40}$ phase at temperatures $T > 4$ K, quite possibly, is associated with the spin–phonon interaction, which leads to a decrease in the Néel temperature, and at a particular critical interaction parameter, the long-range magnetic order vanishes. In this case, the structure retains only the short-range order, which also gives a finite value of the paramagnetic Néel temperature. In order to elucidate the influence of the external magnetic field, the magnetization was measured in the field range -5 T < *H* < 5 T at temperatures $T = 5$ and 300 K. Figure 3 shows the curves of the dependences of the magnetization on the magnetic field for the two-phase compound $0.77Bi_{24}(CoBi)O_{40} \cdot 0.23Co_3O_4$ and the cobalt oxide Co_3O_4. The dependence $M(H)$ for the Co_3O_4 phase in the magnetically ordered state at the temperature $T = 5$ K has a shape typical of polycrystalline antiferromagnets, and at room temperature, a shape typical of paramagnets. The magnetization of the $Bi_{24}(CoBi)O_{40}$ phase was determined by subtracting the magnetiza-

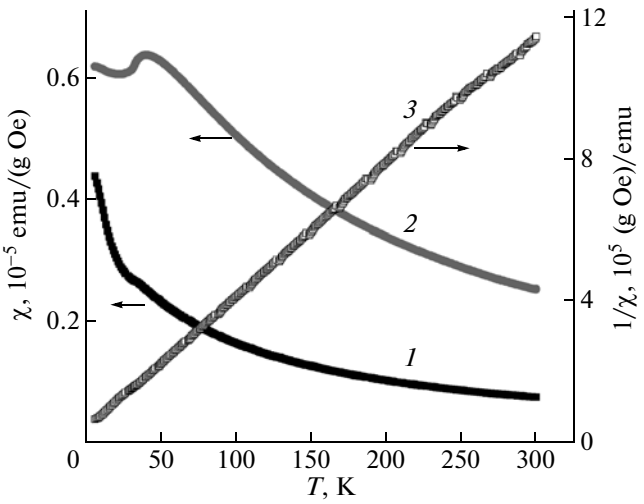

Fig. 2. Temperature dependences of (*1*, *2*) the magnetic susceptibility of (*1*) $0.77Bi_{24}(CoBi)O_{40} \cdot 0.23Co_3O_4$ and (*2*) Co_3O_4 and (*3*) the reciprocal of the magnetic susceptibility of the $Bi_{24}(CoBi)O_{40}$ phase. $H = 5$ T.

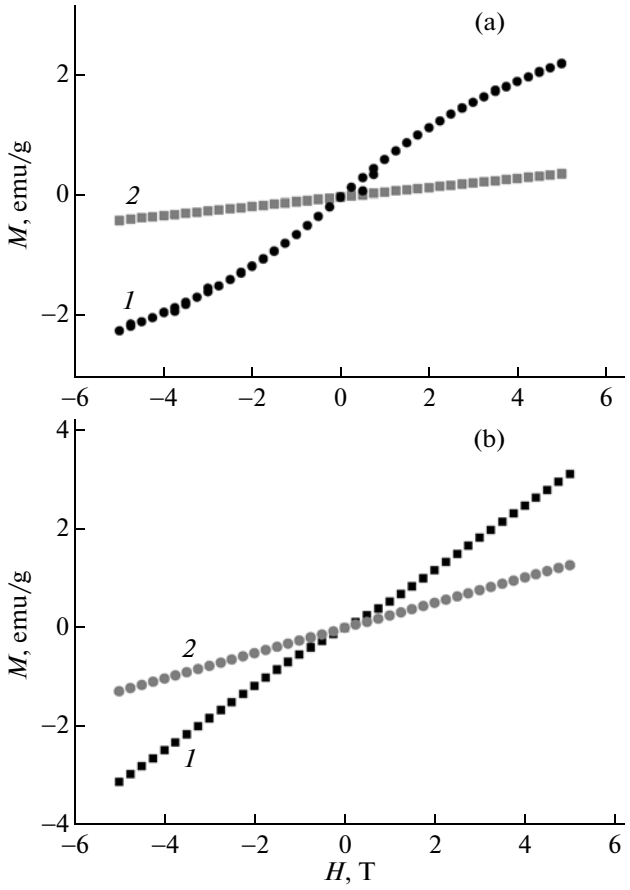

Fig. 3. Field dependences of the magnetization of (a) $0.77Bi_{24}(CoBi)O_{40} \cdot 0.23Co_3O_4$ and (b) Co_3O_4 at temperatures $T = (1)$ 5 and (2) 300 K.

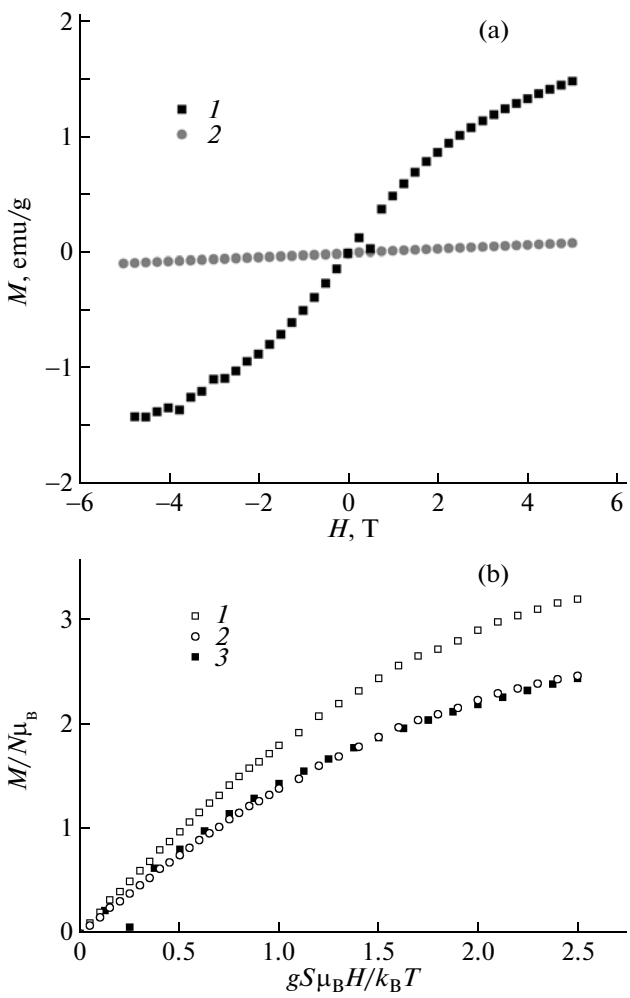

Fig. 4. (a) Magnetization curves $M(H)$ for the $Bi_{24}(CoBi)O_{40}$ compound at temperatures $T = (1)$ 5 and (2) 300 K. (b) Brillouin function $M/N\mu_B = xgSB_S(gS\mu_BH/k_BT)$ plotted for the concentrations of paramagnetic atoms $x = (1)$ 1 and (2) 0.78 versus the magnetic field normalized to the temperature $T = 5$ K, and (3) experimental data for $Bi_{24}(CoBi)O_{40}$.

tion of the two-phase compound from the magnetization of the cobalt oxide: $M[Bi_{24}(CoBi)O_{40}] = M[0.77Bi_{24}(CoBi)O_{40} \cdot 0.23Co_3O_4] - M[0.23Co_3O_4]$. The curves of the magnetic field dependences of the magnetization at temperatures $T = 5$ and 300 K are shown in Fig. 4. At $T = 5$ K, the $Bi_{24}(CoBi)O_{40}$ compound is in the paramagnetic state in a static magnetic field induced by the nearest ferromagnetic planes of the cobalt oxides Co_3O_4. Consequently, one part of the spins of the $Bi_{24}(CoBi)O_{40}$ compound is in a magnetically ordered state, whereas the other part of the spins resides in the paramagnetic state with a weight x. The magnetization in this case is described by the Brillouin function $M/N\mu_B = xgSB_S(gS\mu_BH/k_BT)$, which is presented in Fig. 4b for the spin of the cobalt ion $S = 2$. The difference between the theoretical and experimental results is associated with the magnetic interaction between spins of the two phases of the cobalt oxide and the $Bi_{24}(CoBi)O_{40}$ compound. The fraction of the paramagnetic phase is $x = 0.78$; it is determined by fitting the Brillouin function to the experimental data (Fig. 4b).

The interaction of the spin and elastic subsystems is revealed in the electron paramagnetic resonance (EPR) investigation. The magnetic cobalt ion in both compounds is located in the tetrahedral environment. The temperature dependences of the g-factor and the EPR line width for the $Bi_{24}(CoBi)O_{40}$ phase and the cobalt oxide are shown in Fig. 5. The experimental data have demonstrated that, with an increase in the temperature, the resonance field decreases, whereas the g-factor increases from $g = 2.22$ to 2.25. The observed increase in the g-factor for the cobalt oxide does not currently have an explanation. As regards the $Bi_{24}(CoBi)O_{40}$ compound, the increase in the g-factor, most likely, can be associated with local structural distortions induced by the change in the valence of bismuth, which leads to a reduction of the local symme-

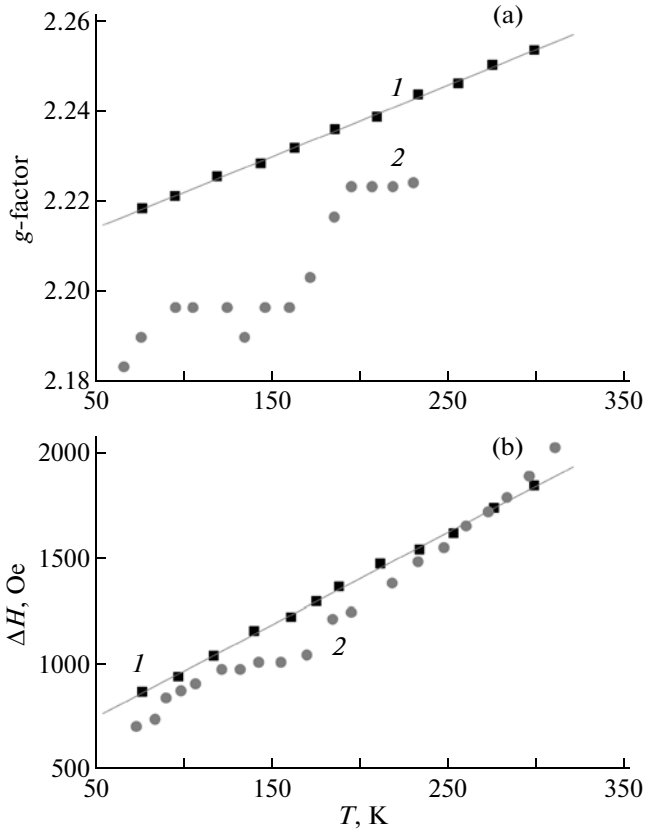

Fig. 5. Temperature dependences of (a) the g-factor and (b) the EPR line width for (*1*) $Bi_{24}(CoBi)O_{40}$ and (*2*) Co_3O_4 [13].

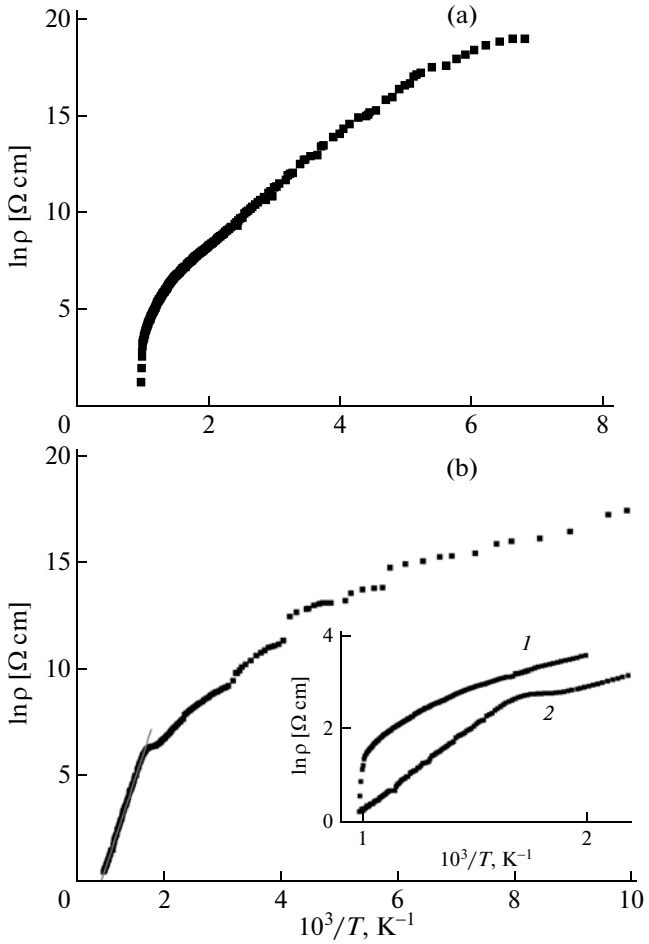

Fig. 6. Logarithm of the electrical resistivity of (a) $0.77Bi_{24}(CoBi)O_{40} \cdot 0.23Co_3O_4$ and (b) Co_3O_4 as a function of the reciprocal of the temperature. The inset shows $\ln\rho(T)$ in the temperature range 500 K < T < 1000 K: (*1*) $0.77Bi_{24}(CoBi)O_{40} \cdot 0.23Co_3O_4$ and (*2*) Co_3O_4.

try. The values of the EPR line width for the two compounds coincide to within 16%. The EPR line width increases linearly with increasing temperature, which indicates the interaction of spins with phonons. For the polycrystalline sample, the EPR line width ΔH is described by the equation $\Delta H = C/T\chi[K(T) + f(\tau)]$ [13], where C is the Curie constant, $K(T)$ is the parameter of the spin–phonon interaction, $f(\tau)$ is the critical contribution in the vicinity of the Néel temperature due to the formation of short-range magnetic order, and $\tau = (T - T_N)/T_N$. For temperatures $T \gg \Theta$, the temperature dependences $\Delta H(T)$ and $K(T)$ coincide. The EPR line shape is slightly asymmetric, so that the line half-widths $\Delta H_1/2$ and $\Delta H_2/2$ on the right and left of the resonance differ by 10 Oe. This difference is within 1% of the line width and stems from the closely spaced resonances of the cobalt spins in Co_3O_4 and $Bi_{24}(CoBi)O_{40}$, for which the difference in the g-factors is also within 1%. The relaxation of the spin moments occurs through the elastic system. The trivalent cobalt ion belongs to the Jahn–Teller ions, and the orbital degeneracy can be removed by the dynamic interaction with the vibrational modes of the tetrahedron or as a result of the orbital ordering of electrons. Each of these factors can lead to anisotropy of the spin–spin correlation functions, and the difference between the g-factor and the value of $g = 2$ is proportional to the exchange anisotropy $\Delta g \sim ((J^z - J^\perp)/J^z)^2$.

4. ELECTRICAL PROPERTIES

The electrical resistivity was measured by the four-probe compensation method at direct current in the temperature range from 77 to 1000 K for two samples of the two-phase compound $0.77Bi_{24}(CoBi)O_{40} \cdot 0.23Co_3O_4$ and the cobalt oxide Co_3O_4. The curve of the temperature dependence of the electrical resistivity for $0.77Bi_{24}(CoBi)O_{40} \cdot 0.23Co_3O_4$ differs significantly from the curve for Co_3O_4 (Fig. 6). The temperature dependence of the electrical resistivity of the phase Co_3O_4 in the temperature range 80 K < T < 600 K has a nonmonotonic behavior (Fig. 6b); in particular, inflections are observed at temperatures $T = 250$ and 170 K; moreover, at the same temperatures, the g-fac-

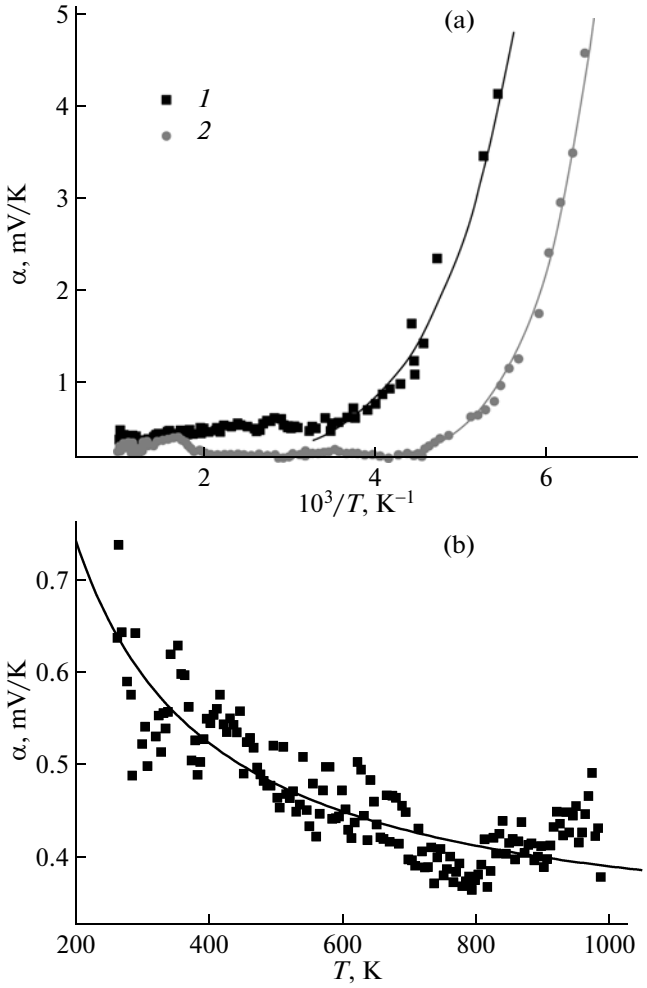

Fig. 7. (a) Temperature dependences of the Seebeck coefficient α: (*1*) $0.77Bi_{24}(CoBi)O_{40} \cdot 0.23Co_3O_4$ and (*2*) Co_3O_4. (b) Fitting function $\alpha = 162/T + 0.00027T$ (solid line) of the temperature dependence of the thermoelectric power for $0.77Bi_{24}(CoBi)O_{40} \cdot 0.23Co_3O_4$ (points).

tor changes abruptly. These anomalies can be attributed either to the formation of structural distortions in the crystal lattice or to the removal of the degeneracy of the vibrational modes of the octahedron due to the electron–phonon interaction. At the temperature $T =$ 600 K, most probably, there occurs a transition from the low-spin state to the high-spin state with possible charge fluctuations $2Co^{3+} = Co^{2+} + Co^{4+}$ [14], which form an electron-hole pair that leads to a change in the activation energy $\Delta E = 0.31$ eV. At temperatures in the range 520 K $< T <$ 600 K, the temperature dependence of the electrical resistivity of the cobalt oxide has a small plateau, which is not observed in the dependence of the two-phase compound. The behavior of the electrical resistivity of the two-phase compound $0.77Bi_{24}(CoBi)O_{40} \cdot 0.23Co_3O_4$ is adequately described by the exponential relationship in the temperature range 200 K $< T <$ 750 K with the activation energy $\Delta E = 0.23$ eV. With a further increase in the temperature, the electrical resistivity $\rho(T)$ of the $0.77Bi_{24}(CoBi)O_{40} \cdot 0.23Co_3O_4$ compound decreases abruptly and, in the temperature range 900 K $< T <$ $T^* = 950$ K, is fairly well described by the power function $\ln\rho = A(1 - T/T^*)^{0.23}$, whereas the cobalt oxide is characterized by the linear dependence of $\ln\rho$ on the reciprocal of the temperature. The electrical resistivity of Co_3O_4 is two orders of magnitudes lower than that of $0.77Bi_{24}(CoBi)O_{40} \cdot 0.23Co_3O_4$ at temperatures $T <$ 1000 K (see inset to Fig. 6b).

The temperature dependences of the Seebeck coefficient for the two compounds under investigation are shown in Fig. 7a. The dependences $\alpha(T)$ are qualitatively different in the high-temperature range 300 K $<$ $T <$ 1000 K. In particular, the thermoelectric power of Co_3O_4 increases during heating at temperatures $T >$ 350 K and reaches a maximum at $T = 610$ K, whereas the thermoelectric power of the two-phase compound decreases with increasing temperature to $T = 800$ K. At $T < 250$ K, the temperature dependences of the thermoelectric power of $0.77Bi_{24}(CoBi)O_{40} \cdot 0.23Co_3O_4$ and Co_3O_4 are qualitatively similar, and the experimental data are adequately described by the exponential relationship $\alpha(T) = A\exp(\Theta_0/k_BT)$, where Θ_0 is the energy of the optical mode, which for these compounds is determined by the collective vibrational modes of the tetrahedra with $\Theta_0 = 0.092$ eV for $0.77Bi_{24}(CoBi)O_{40} \cdot 0.23Co_3O_4$ and $\Theta_0 = 0.12$ eV for Co_3O_4. The large values of the thermoelectric power at low temperatures are associated with the electron–phonon drag effect. The cobalt ions are characterized by charge fluctuations between orbitals. This leads to a strong interaction with the internal polarization field induced by optical vibrations as compared to the interaction associated with the deformation potential. The temperature dependence $\alpha(T)$ is determined by the temperature dependences of the phonon and electron (hole) relaxation times. The interaction of holes with long-wavelength acoustic phonons leads to the power relationship $\alpha(T) \sim T^{-3.5}$ [15], which manifests itself in semiconductors in the low-temperature range (50–100 K). The interaction of holes with optical phonons is significant at higher temperatures. For $k_BT < \Theta_0/4$, the number of these phonons in the vibrational spectrum exponentially decreases $n_q \sim \exp(-\Theta_0/k_BT)$. The relaxation time of charge carriers in the optical mode is inversely proportional to the number of phonons $\tau \sim 1/n_q$; therefore, we can expect that the thermoelectric power will be adequately described by the exponential relationship $\alpha(T) = A\exp(\Theta_0/k_BT)$ [15]. At higher temperatures $T > 250$ K, the thermoelectric power is governed by the electrons and described by the relationship $\alpha(T) = k_B/e(\Delta E/k_BT + \gamma k_BT)$ [16], where e is the elementary charge, k_B is the Boltzmann constant, γk_BT is the average energy carried by holes, and ΔE is the activation energy for hopping conduction.

Figure 7b shows the fitting function $\alpha(T) = A/T + BT$ with $A = 162$ V and $B \approx 0.0003$ V/K. Using this function, we determined the activation energy $\Delta E = 0.160 \pm 0.015$ eV and the average kinetic energy of charge carriers (holes) of the order 10^{-3} eV. In the temperature range 250 K < T < 800 K, the thermoelectric power decreases monotonically and reaches a minimum at the temperature $T = 800$ K for $0.77Bi_{24}(CoBi)O_{40} \cdot 0.23Co_3O_4$. According to the theoretical results, the thermoelectric power has a minimum at the temperature $T_{min} = \Delta E\sqrt{3(\pi - 2)/2\pi^2}$ for hopping conduction over the nearest neighbors under the condition $k_B T \ll \mu_0$ (μ_0 is the chemical potential) [17]. The activation energy found from the temperature of the minimum is $\Delta E = 0.17$ eV. A similar temperature dependence of the thermoelectric power was observed in samples of $Fe_3O_{4-x}F_x$ with hopping conduction [18], where the activation energy determined from the minimum of the dependence $\alpha(T)$ is equal to $\Delta E = 0.04$ eV and has a smaller value as compared to the value $\Delta E = 0.076$ eV obtained from the temperature dependence of the electrical conductivity. Thus, at temperatures $T \sim 250$ K, the thermoelectric power is characterized by a crossover from the phonon mechanism to the electron mechanism.

A correlation between the structural characteristics and the kinetic coefficients can be traced in terms of the thermal expansion coefficient of the samples. The temperature dependences of the volume thermal expansion coefficient β for the two compounds under investigation are shown in Fig. 8. It can be clearly seen from this figure that the volume thermal expansion coefficient for the cobalt oxide Co_3O_4 [14] is two times smaller than that for the $Bi_{24}(CoBi)O_{40}$ compound at room temperature. An increase in the temperature of the sample leads to a monotonic increase in the lattice parameters of the cobalt oxide Co_3O_4 with the subsequent drastic increase at higher temperatures $T >$ 700 K [14]. This effect is also explained by the intraatomic spin transition in the cobalt ion inside the octahedron from the low-spin (LS) ground state of the electronic configuration to the high-spin (HS) state due to the change in the ionic radius of cobalt from $R_{LS} = 0.053$ nm to $R_{HS} = 0.061$ nm [19]. The lattice of the $Bi_{24}(CoBi)O_{40}$ compound expands to the temperature $T = 630$ K, and the volume thermal expansion coefficient β has a local minimum at $T = 700$ K. The observed increase in the thermal expansion coefficient of the $Bi_{24}(CoBi)O_{40}$ compound, quite possibly, is associated with the increase in the radius of the cobalt ion in the tetrahedron as a result of the redistribution of the electron density between the t_{2g} and e_g states. A change in the charge state of the bismuth ions causes a decrease in the ionic radius of Bi^{4+} and, correspondingly, leads to a decrease in the linear size of the lattice.

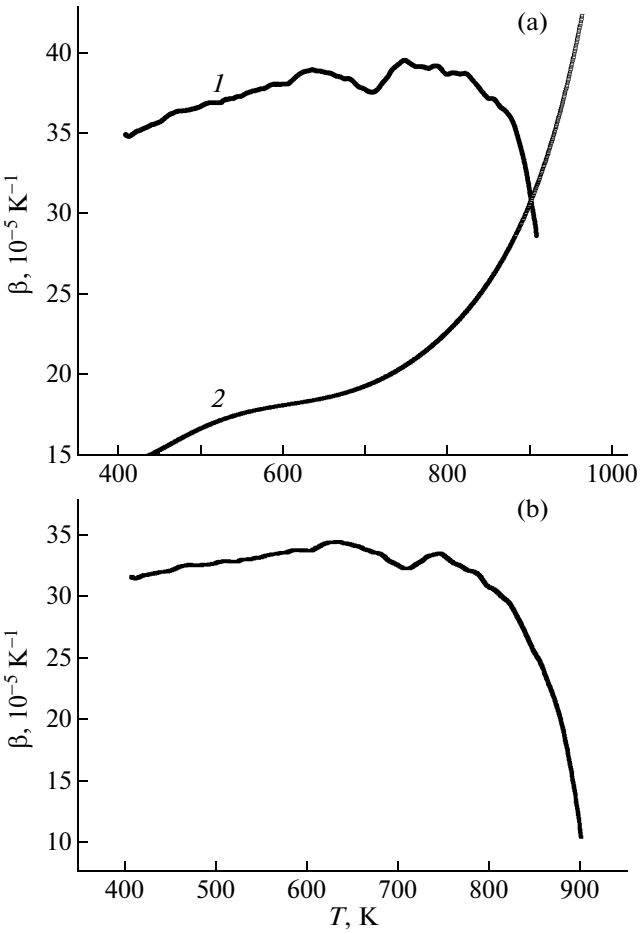

Fig. 8. Temperature dependences of the thermal expansion coefficient β for (a) (*1*) $0.77Bi_{24}(CoBi)O_{40} \cdot 0.23Co_3O_4$ and (*2*) Co_3O_4 and (b) the $Bi_{24}(CoBi)O_{40}$ phase.

5. THE MODEL

Let us consider the scheme of the arrangement of the bismuth ions responsible for the formation of an electronic-structure phase transition in one of the planes (Fig. 9). The pentavalent bismuth ion is surrounded by eight trivalent bismuth ions. The transition of an electron from the Bi^{3+} ion to the Bi^{5+} ion can be interpreted as the formation of a localized exciton in the cubic lattice site. For the electron transition between the lattice sites, it is necessary that the charge state should be changed from Bi^{4+} to Bi^{3+}. We use a simple model with two sites: one site is occupied by the Bi^{3+} ion with the filled 6*s* shell, while the other site is occupied by the Bi^{5+} ion with the empty 6*s* shell, so that, on the average, there is one electron per site with a charge carrier concentration n_l. The redistribution of the charges $Bi^{3+} + Bi^{5+} = Bi^{4+} + Bi^{4+}$ between the adjacent sites results in the transition of two electrons to the conduction band in which the electron concentration is n_s. These processes obey the law of conservation of charge: $n_l + n_s = 1$. We take into account the

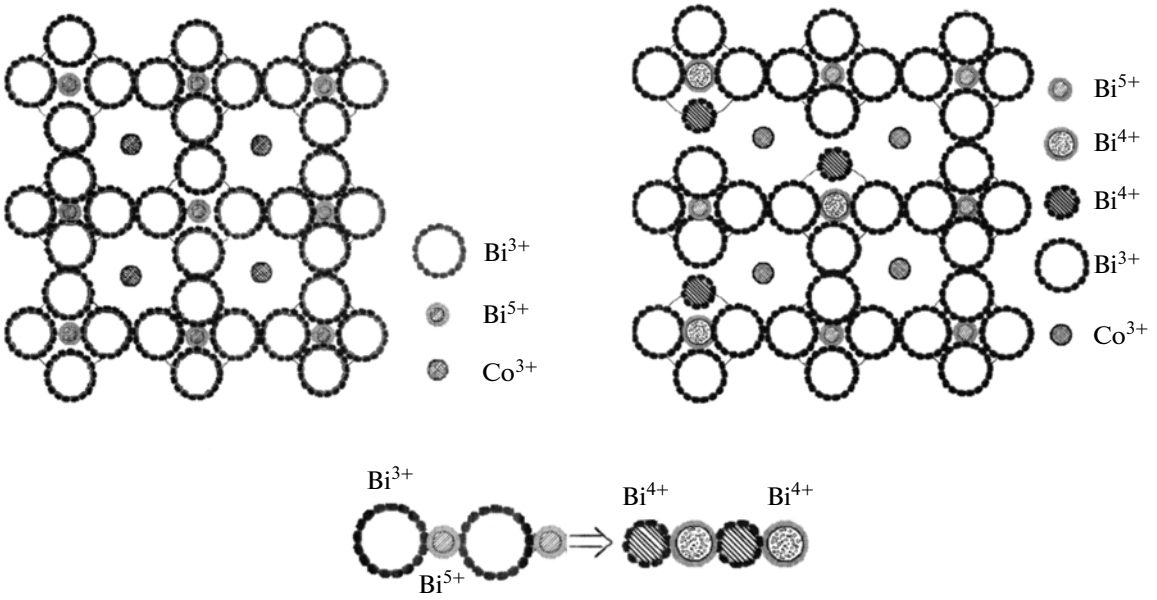

Fig. 9. Scheme of the arrangement of the bismuth and cobalt ions in the crystal lattice of the $Bi_{24}(CoBi)O_{40}$ compound.

Coulomb interaction between electrons in the form $Gn_l n_s = G(1 - n_s)n_s$; then, the energy of the system can be represented as a function of the number of itinerant band electrons $n_s = 1 - n_l$. The contribution to the energy of the system from the kinetic energy of the *s* electrons filling the lower states of the *s* band can be represented in the form $Wn^{5/3}$ [20], and the exchange energy can be written as $Jn^{4/3}$. In this case, the energy of the electronic system can be represented in the following form [21]:

$$F_e = E_g n - Jn^{4/3} + Wn^{5/3} - Gn^2$$
$$- T(n\ln n - (1-n)\ln(1-n)),$$

where $E_g = E_0 - G$; E_0 is the energy of electrons in bismuth ions, which is measured from the bottom of the conduction band; W is the kinetic energy; and the last term corresponds to the entropy contribution to the free energy.

At the absolute zero of the temperature, an increase in the concentration of charge carriers in the conduction band can lead to a first-order phase transition. The experimental data indicate a strong correlation between the electronic and structural characteristics. Therefore, in addition to the electron–electron interaction, the model should take into account the electron–lattice interaction [22]. This is associated with the fact that ions of different valences, between which the transition occurs, have strongly different (by 15–20%) ionic radii. Accordingly, the electronic phase transition is usually accompanied by a significant change in the lattice parameters. The electron–lattice interaction includes the interaction of electrons with a homogeneous deformation and with phonons at a specified strain. In the self-consistent field approximation, we take into account the interaction of electrons with a homogeneous deformation in the linear approximation for the displacement of the ion. The complete expression for the free energy has the following form: $F = F_e - \lambda n_s u + 1/2ku^2$, where λ describes the electron–lattice interaction and k is the elastic constant of the lattice.

The dependence of the relative displacement of the ion and the concentration of electrons in the conduction band on the temperature can be determined by minimizing the free energy in two parameters: $dF/du = 0$ and $dF/dn = 0$. As a result, we obtain the transcendental equation, the solution of which for the concentrations n_s is adequately described by the exponential dependence on the reciprocal of the temperature (see inset to Fig. 10). For the exchange interaction $J = 900$ K, the calculated activation energy $\Delta E = 0.21$ eV agrees satisfactorily with the experimental value $\Delta E = 0.23$ eV obtained from the electrical conductivity of the two-phase compound $Bi_{24}(CoBi)O_{40} \cdot 0.23Co_3O_4$ (Fig. 6). The change in the lattice parameters as a function of the temperature is determined by two competing factors: the anharmonicity of vibrations of the ions in the lattice, which are responsible for the lattice expansion $u_a = b/2k^2$ (where b is the elastic constant of the cubic term in the displacement of the ion), and the compression of the lattice due to the electron–lattice interaction $u_c = \lambda n_s/k$. The resulting displacement of the ions $u = b/2k^2 - \lambda n_s/k$ is presented in Fig. 11. The thermal expansion coefficient was calculated from the derivative of the displacement of the ions with respect to the temperature du/dT (see

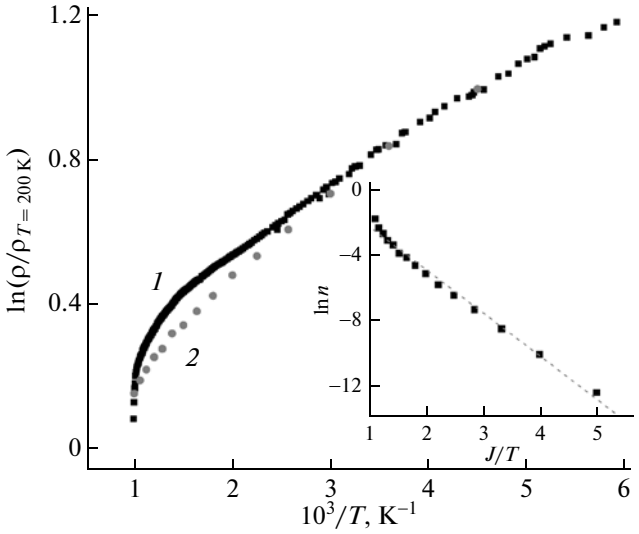

Fig. 10. Logarithm of the electrical resistivity normalized to the electrical resistivity at $T = 200$ K as a function of the reciprocal of the temperature: (*1*) experiment and (*2*) theoretical calculation. The inset shows the logarithm of the concentration of electrons in the conduction band as a function of the reciprocal of the temperature, calculated by minimizing the free energy for the parameters $E/J = 2.5$, $W/J = 3$, $G/J = 0.6$, $\lambda/J = 0.5$, and $k/J = 6$.

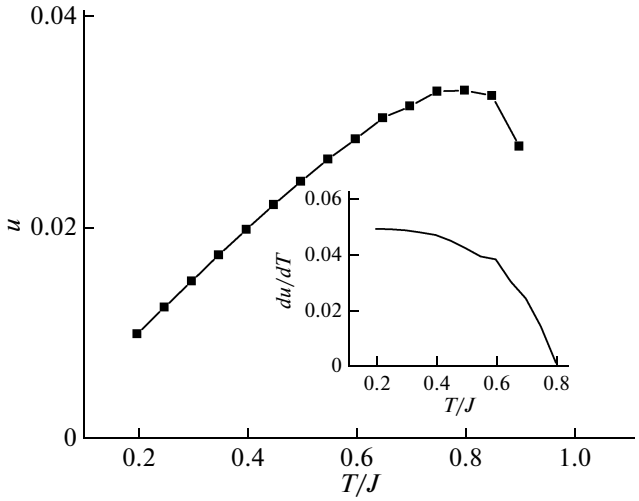

Fig. 11. Temperature dependence of the relative displacement of ions $u = b/2k^2 - \lambda n_s/k$. The inset shows the derivative of the displacement of the ions with respect to the temperature du/dT, calculated by taking into account the temperature dependence of the concentration of electrons in the conduction band for the parameters $E/J = 2.5$, $W/J = 3$, $G/J = 0.6$, $\lambda/J = 0.5$, $k/J = 6$, and $b/J = 1$.

inset to Fig. 11). The calculated temperature dependence of the derivative of the displacement of the ions $du/dT(T)$ is qualitatively consistent with the experimental data.

6. CONCLUSIONS

Thus, the results obtained have demonstrated that, in the $Bi_{24}(CoBi)O_{40}$ compound containing the bismuth ions Bi^{5+} and Bi^{3+} with the filled and empty 6*s* shells, the magnetic properties are determined by the cobalt ions with weak antiferromagnetic interaction. It has been found that, in the paramagnetic state, there is a strong spin–phonon interaction, which leads to an increase in the EPR line width. The activation type of electrical conduction with positively charged carriers (holes) has been established. A crossover of the thermoelectric power from the phonon mechanism to the electron mechanism during heating of the sample has been revealed and a monotonic increase in the thermoelectric power at temperatures $T > 800$ K has been observed. The thermal expansion coefficient of the bismuth cobaltite abruptly decreases in the temperature range $T > 800$ K. It has been found that there is a correlation of the electrical and structural properties of the solid solution at temperatures in the range $T = 800$–1000 K. A model has been proposed for the redistribution of charges between bismuth ions with variations in the ionic radii and the lattice parameter without a change in the lattice symmetry. The concentrations of electrons in the conduction band and the displacements of ions, the temperature dependences of which are qualitatively consistent with the thermal expansion coefficient of the lattice, have been calculated within the model of electrons interacting with the lattice in the self-consistent molecular field approximation.

ACKNOWLEDGMENTS

We would like to thank G.S. Patrin for his assistance in performing the magnetic measurements and A.V. Vorotynov for performing the electron paramagnetic resonance measurements and helpful discussions of the experimental results.

This study was supported by the Russian Foundation for Basic Research (project nos. 09-02-92001-NNS_a, 12-02-00125-a, and 11-02-98004-r_sibir'_a).

REFERENCES

1. A. Sadoc and B. Mercey, Phys. Rev. Lett. **104**, 046804 (2010).
2. F. Massee, S. de Jong, Y. Huang, W. K. Siu, I. Santoso, A. Mans, A. T. Boothroyd, D. Prabhakaran, R. Follath, A. Varykhalov, L. Patthey, M. Shi, J. B. Goedkoop, and M. S. Golden, Nat. Phys. **7**, 978 (2011).
3. K. Yamauchi, Phys. Rev. B: Condens. Matter **79**, 212404 (2009).
4. A. A. Fursina, R. G. S. Sofin, I. V. Shvets, and D. Natelson, Phys. Rev. B: Condens. Matter **81**, 045123 (2010).
5. C.-S. Cheng, M. Serizawa, H. Sakata, and T. Hirayama, Mater. Chem. Phys. **53**, 225 (1998).

6. R. Metselaar, R. E. J. van Tol, and P. Piercy, J. Solid State Chem. **38**, 335 (1981).
7. N. Rangavital, T. N. Guru Row, and C. N. R. Rao, Eur. J. Solid State Inorg. Chem. **31**, 409 (1994).
8. Y. Ikedo, J. Sugiyama, H. Nozaki, H. Itahara, J. H. Brewer, E. J. Ansaldo, G. D. Morris, D. Andreica, and A. Amato, Phys. Rev. B: Condens. Matter **75**, 054424 (2007).
9. L. A. Solovyov, J. Appl. Crystallogr. **37**, 743 (2004).
10. G. A. Komandin, V. I. Torgashev, A. A. Volkov, O. E. Porodinkov, I. E. Spektor, and A. A. Bush, Phys. Solid State **52** (4), 734 (2010).
11. A. Maitre, M. Francois, and J. C. Gashon, J. Phase Equilib. Diffus. **25**, 59 (2004).
12. S. Angelov, E. Zhecheva, R. Stoyanova, and M. Atanasov, J. Phys. Chem. Solids **51**, 1157 (1990).
13. P. Dutta, M. S. Seehra, S. Thota, and J. Kumar, J. Phys.: Condens. Matter **20**, 015218 (2008).
14. D. Broemme, Doctor Thesis (Technische Universität Eindhoven, Eindhoven, Germany, 1990).
15. F. J. Blatt, *Physics of Electronic Conduction in Solid* (McGraw-Hill, New York, 1968).
16. V. L. Bonch-Bruevich, I. P. Zvyagin, R. Kaiper, A. G. Mironov, R. Enderlein, and B. Esser, *Electronic Theory of Disordered Semiconductors* (Nauka, Moscow, 1981) [in Russian].
17. O. E. Parfenov and F. A. Shklyaruk, Semiconductors **41** (9), 1021 (2007).
18. H. Graener, M. Rosenberg, T. E. Whall, and M. R. Jones, Philos. Mag. **40**, 389 (1979).
19. V. A. M. Brabers and A. D. D. Broemme, J. Magn. Magn. Mater. **104–107**, 405 (1992).
20. L. M. Khriplovich, E. V. Kholopov, and I. E. Paukov, J. Chem. Thermodyn. **14**, 207 (1982).
21. E. Vusher and R. G. Maines, Solid State Commun. **11**, 1441 (1972).
22. D. I. Khomskii, Sov. Phys.—Usp. **22** (10), 879 (1979).

Translated by O. Borovik-Romanova